

Microfluidic directional emission control of an azimuthally polarized radial fibre laser

Alexander M. Stolyarov^{1,2,3}, Lei Wei^{1,2}, Ofer Shapira^{1,2}, Fabien Sorin^{1,2†}, Song L. Chua^{1,4}, John D. Joannopoulos^{1,2,5} and Yoel Fink^{1,2,6*}

Lasers with cylindrically symmetric polarization states are predominantly based on whispering-gallery modes^{1–7}, characterized by high angular momentum and dominated by azimuthal emission. Here, a zero-angular-momentum laser with purely radial emission is demonstrated. An axially invariant, cylindrical photonic-bandgap fibre cavity⁸ filled with a microfluidic gain medium plug is axially pumped, resulting in a unique radiating field pattern characterized by cylindrical symmetry and a fixed polarization pointed in the azimuthal direction. Encircling the fibre core is an array of electrically contacted and independently addressable liquid-crystal microchannels embedded in the fibre cladding. These channels modulate the polarized wavefront emanating from the fibre core, leading to a laser with a dynamically controlled intensity distribution spanning the full azimuthal angular range. This new capability, implemented monolithically within a single fibre, presents opportunities ranging from flexible multidirectional displays to minimally invasive directed light delivery systems for medical applications.

Rotationally symmetric resonators capable of omnidirectional emission in the direction perpendicular to the axis of symmetry have been investigated in a number of recent studies^{1–7}. These cylindrically symmetric sources rely on the excitation of whispering-gallery modes (Fig. 1b), confined near the cavity boundary by total internal reflection. Light escapes these resonators only through diffraction losses or scattering from surface roughness, thus limiting control over the output coupling. Here, we report on a cylindrical photonic-bandgap (PBG) fibre cavity that supports purely radial modes (Fig. 1a). In principle, this structure allows full control over output coupling and the potential for a reduction in volume without compromising the quality factor, Q . Additionally, the shorter cavity length of these radial modes could allow for a larger free spectral range and consequently higher finesse than whispering-gallery modes. Importantly, the radially directed emission from the extended cylindrical surface of this fibre laser differs from the axial emission characteristic of conventional Bragg fibre lasers^{9,10} and planar annular Bragg resonators^{11–14}.

The fibre fabrication method is based on the thermal drawing of a macroscopic preform (Fig. 2a) assembled with all the solid materials and geometry of the resulting fibre (see Methods for details)¹⁵. The preform consists of a hollow annular multilayered cavity comprised of a 35-layer structure of chalcogenide glass ($\text{As}_{25}\text{S}_{75}$) and polycarbonate¹⁶. (The presence of the surface seam was neglected in our analysis because of its small dimension relative

to the core size.) Further out in the polycarbonate cladding are several pairs of conductive carbon-loaded polyethylene (CPE) electrodes that flank hollow channels. The composite structure is drawn under a high-stress regime ($\sim 400 \text{ g mm}^{-2}$), yielding an

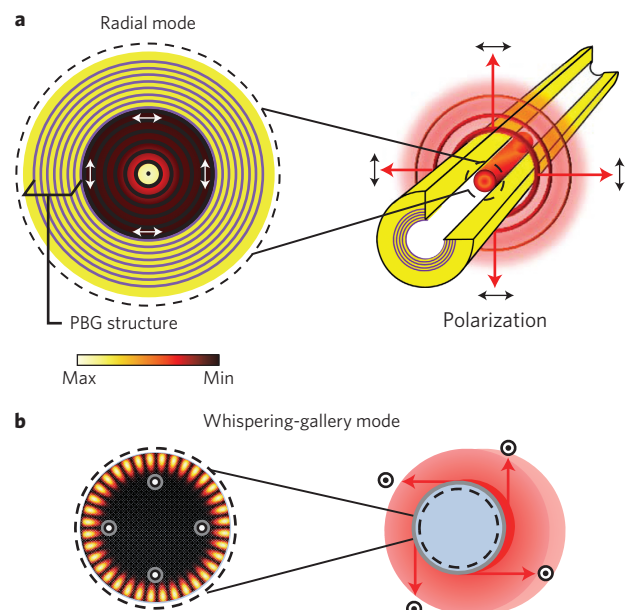


Figure 1 | Comparison of radial and whispering-gallery modes. a, Schematic drawing of the radially emitting fibre laser structure and energy density plot for a high- Q TE_{0n} fibre cavity laser mode. The outgoing, radially directed red arrows denote the direction of laser emission. The white arrows overlaid on the energy density plot denote the polarization of the mode, which is also indicated in black arrows outside the cavity in the schematic. The periodic PBG structure surrounding the fibre core corresponds to layers of $\text{As}_{25}\text{S}_{75}$ (purple) and polycarbonate (yellow). **b**, Schematic drawing of a cylindrical structure that supports high- Q whispering-gallery modes. The primarily azimuthally directed red arrows denote the tangential laser emission of the high-angular-momentum modes. The energy density plot corresponds to a high-order whispering-gallery mode supported by the cylindrical structure shown in blue. The polarization of this mode is indicated by the white dots overlaid on the energy density plot and the black dots on the schematic. Note: the colour key indicated in the figure applies to energy density plots in both **a** and **b**.

¹Research Laboratory of Electronics, Massachusetts Institute of Technology, 77 Massachusetts Avenue, Cambridge, Massachusetts 02139, USA, ²Institute for Soldier Nanotechnologies, Massachusetts Institute of Technology, 77 Massachusetts Avenue, Cambridge, Massachusetts 02139, USA, ³School of Engineering and Applied Sciences, Harvard University, 29 Oxford Street, Cambridge, Massachusetts 02138, USA, ⁴Department of Electrical Engineering and Computer Science, Massachusetts Institute of Technology, 77 Massachusetts Avenue, Cambridge, Massachusetts 02139, USA, ⁵Department of Physics, Massachusetts Institute of Technology, 77 Massachusetts Avenue, Cambridge, Massachusetts 02139, USA, ⁶Department of Materials Science and Engineering, Massachusetts Institute of Technology, 77 Massachusetts Avenue, Cambridge, Massachusetts 02139, USA; [†]Present address: Laboratoire surface du verre et interfaces, Unité Mixte CNRS/Saint-Gobain UMR 125, 39 quai Lucien Lefranc, 93303 Aubervilliers, France. *e-mail: yoel@mit.edu

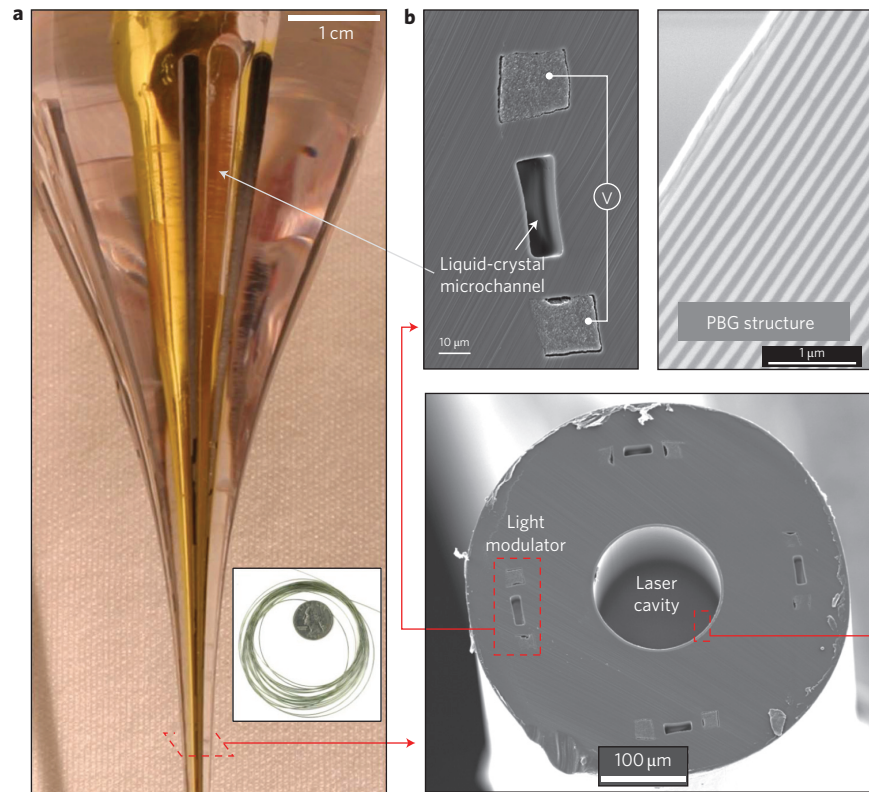


Figure 2 | Preform and fibre structure. **a**, Photograph of the drawn preform. The black strips are the CPE electrodes. The orange reflection from the $As_{25}S_{75}$ glass is seen in the centre of the structure. Inset: several metres of fibre is coiled around a US quarter. **b**, Bottom: scanning electron microscope image of the multimaterial fibre device (scale bar, $100\ \mu\text{m}$). The fibre core is surrounded by four light modulators. Top left: enlarged view of the CPE electrodes flanking a hollow microchannel, which is filled with liquid crystal post draw (scale bar, $10\ \mu\text{m}$). Top right: enlarged view of the multilayer structure forming the PBG cavity (scale bar, $1\ \mu\text{m}$). The white and grey layers correspond to $As_{25}S_{75}$ and polycarbonate, respectively.

axially invariant, rotationally symmetric, PBG fibre cavity with a transmission bandgap centred near $550\ \text{nm}$ and a bilayer periodicity of $160\ \text{nm}$ (Fig. 2b, top right). The fibre core is surrounded by four electrically addressable microfluidic channels embedded in the fibre cladding (Fig. 2b, bottom). The challenge in drawing such a structure that is reduced in size by a factor of 100 lies in maintaining the integrity and symmetry of the multilayers down to the final scale while preventing the deformation of the hollow channels and electrodes.

Recent studies have demonstrated optofluidic fibre devices with dynamically tunable properties^{17,18}. In this work, a microfluidic pump (shown in Fig. 3a and described in the Methods) is used to transport organic-dye-doped water plugs inside the fibre core. The internal surface of the fibre core is hydrophobic and not wet by the aqueous plug, which remains intact during rapid movement at velocities of $35\ \text{mm s}^{-1}$ (Fig. 3b). The pressure field is mediated through a transparent and immiscible fluid (for example, silicone oil), allowing reversible transport of the lasing plug to any position within the fibre (Fig. 3b,c).

The laser wavefront emitted from the fibre core appears as an axially collimated ring-like beam in the far field (Fig. 4a). The axial collimation results from the low diffraction facilitated by the smooth interfaces of the water plug, and the continuous translational symmetry of the laser cavity along the fibre axis. The penetration depth of the pump beam, combined with the circular cross-section of the core, defines a cylinder from which laser light is emitted. (Note that the actual plug length, which is on the order of a centimetre, does not influence the laser emission.) For the $1\ \text{mM}$ Rhodamine 590 (R590) water plug used in our experiments, the penetration depth is $\sim 100\ \mu\text{m}$. The axial divergence angle,

which is proportional to the ratio between the wavelength and the penetration depth, is therefore expected to be $\sim 10\ \text{mrad}$.

The cylindrical symmetry of the emission stems from the isotropic fluorescence of the dye and its coupling to the fibre cavity modes. Below threshold, the measured isotropic and unpolarized spontaneous emission populates all the available fibre modes. However, above threshold, a purely azimuthally polarized beam emerges from the PBG fibre cavity (Fig. 4b), which indicates coupling to specific low-threshold fibre modes. These modes are the high-Q TE_{0n} modes, with an electric field polarization identical to what we measure in the radial laser emission. This isotropic emission is in contrast to the anisotropic emission observed from dye-doped solid plugs¹⁹. In a low-viscosity solvent such as water, fluorescence randomization occurs due to the fast molecular reorientation of the dye, which happens on a picosecond scale²⁰, much faster than the nanosecond scale of the fluorescence lifetime²¹. Fluorescence anisotropy is not therefore expected, which is consistent with our experimental observations.

A $1\ \text{mM}$ R590-doped water plug was introduced into the fibre core and pumped by a linearly polarized Nd:YAG laser at $532\ \text{nm}$ (see Methods for details). A typical measurement depicting the dependence of output energy on input energy shows a clear threshold at $165\ \text{nJ}$ (Fig. 4c). The spacing between individual lasing peaks reveals an average separation of $1.78\ \text{nm}$ for a fibre with an $80\ \mu\text{m}$ core (Fig. 4d). Considering the free spectral range of the longitudinal modes in a Fabry–Perot resonator, $\Delta\lambda \approx \lambda_0^2/2nd$, where λ_0 is the central lasing wavelength and n is the refractive index of the dye solution ($n = 1.33$), a cavity length $d = 78\ \mu\text{m}$ is calculated, which agrees well with the fibre core diameter and further confirms the radial nature of the emission.

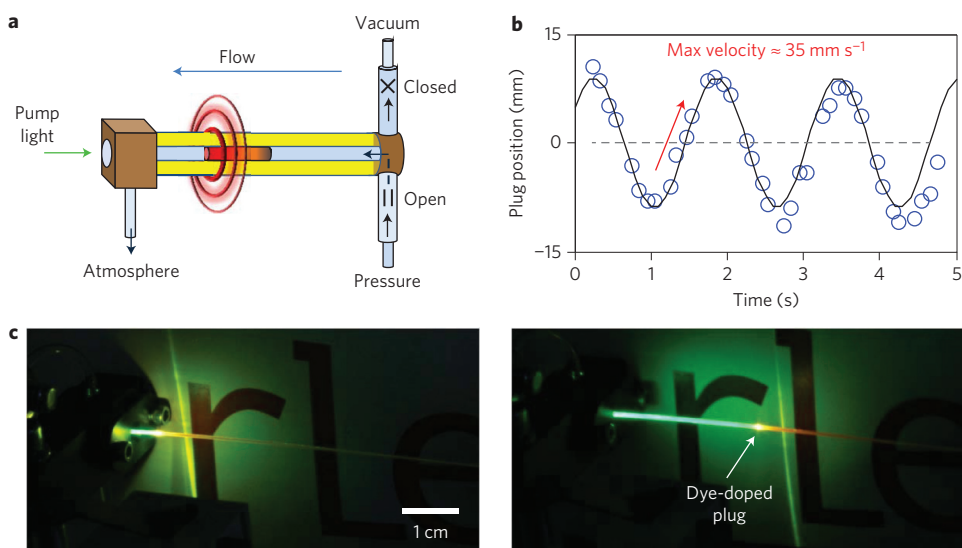


Figure 3 | Microfluidic laser system. **a**, Schematic of the microfluidic system used to transport the gain medium plug within the fibre core. The system is composed of an optical/fluidic coupler at the input facet of the fibre and a set of pressure-driven, electrically actuated microdispensing valves at the distal end, allowing for bidirectional flow control. Silicone oil (refractive index, $n = 1.38$) is in light blue and the organic dye-doped water plug (refractive index, $n = 1.33$) is the red cylinder. **b**, The dynamics of the system is recorded as the plug is optically pumped and simultaneously set into an oscillating motion by alternating the valve actuations. Blue circles correspond to measured plug position. The black curve is a sinusoidal fit to the data. Plug velocities up to 35 mm s^{-1} are achieved before the drop disperses into two or more fragments. **c**, Photographs of the lasing plug at two different positions along the fibre. The radially emitted laser light is seen scattering from a screen with an 'rle' logo positioned behind the fibre. (The green pump light is also seen along the fibre axis. This is due to the transmission bandgap shift, which arises from filling the core with the silicone oil³⁰).

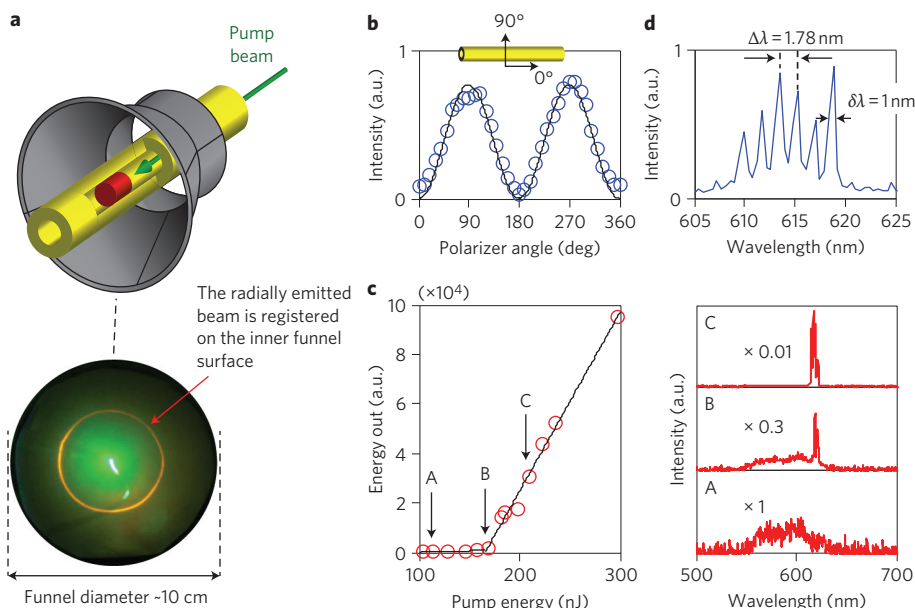


Figure 4 | Laser characterization. **a**, Top: schematic of the fibre laser threaded through a funnel, the surface of which is used to register the radially emitted wavefront. The red cylinder in the fibre core is an R590-doped water plug. Bottom: image of the fibre threaded through the funnel. The radially emitted light emanating from the dye-doped plug is seen as a ring-like pattern scattered from the inner surface of the funnel. The green light at the centre is from the pump beam. **b**, Polarization of the radial laser light emitted from the fibre, measured by rotating a linear polarizer in the plane shown by the vectors in the inset. **c**, Left: output energy dependence on pump energy for a R590-doped water plug showing a threshold of 165 nJ. Right: spectra measured from the fibre laser below threshold (A), near threshold (B) and above threshold (C). **d**, Resolved spectra from the emission of an $80 \mu\text{m}$ core fibre just above laser threshold. The measured quality factor, given by $Q = \lambda_0 / \delta\lambda$ (where $\delta\lambda$ is the spectral width of a given mode) is ~ 615 ; this is lower than expected from theory, due to the limited resolution of the measurement set-up and a non-ideal fibre structure.

So, how can we use the intrinsic radial emission and azimuthal polarization state to achieve a useful effect? The problem of directing coherent light is recognized as an important one for a variety of applications. Current solutions can be classified into those that

make use of moving mechanical parts and those that rely on non-mechanical mechanisms^{22–27}. Although having advantages such as high angular precision, the non-mechanical solutions are nevertheless constrained to a narrow angular range. Here, we demonstrate an

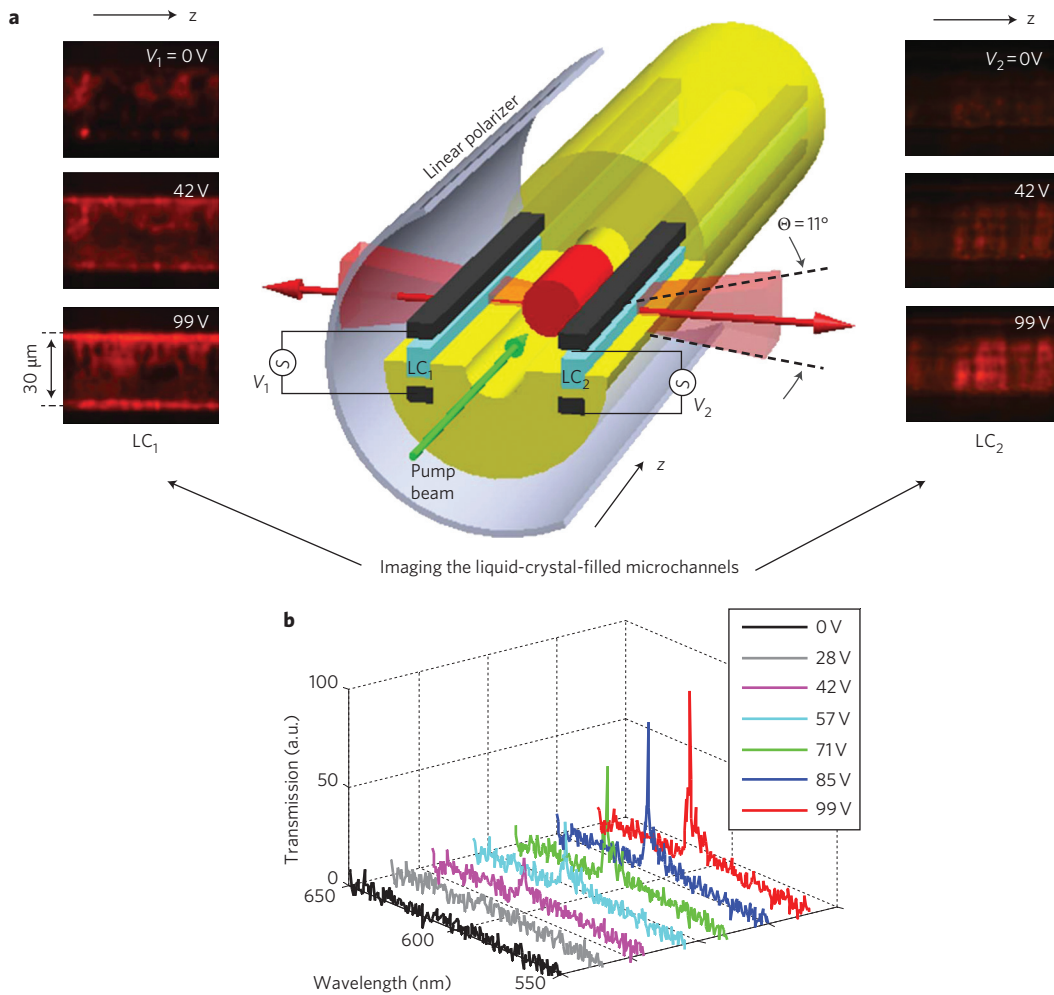


Figure 5 | Azimuthally controlled laser emission. **a**, Schematic of the fibre device depicting the simultaneous control of two oppositely facing liquid-crystal-filled microchannels, labelled LC₁ and LC₂. Light blue strips correspond to liquid-crystal-filled microchannels and black strips to in-fibre electrodes (Fig. 2). V₁ and V₂ are the voltages applied to the electrode pairs that flank LC₁ and LC₂, respectively. The transmission axis of the linear polarizer that surrounds the fibre points along the z-axis. The liquid-crystal microchannels have widths of 30 μm , and are located 160 μm from the fibre centre (Fig. 2b), leading to an angular resolution of $\sim 11^\circ$ for this structure. Left and right: instead of recording the far-field laser intensity as in Fig. 4a, here we directly image the laser light at the plane of the liquid-crystal-filled microchannels as the applied voltages V₁ and V₂ are varied. The light intensity passing through LC₁ (LC₂) does not change as a function of the voltage V₂ (V₁), demonstrating the independent control available in each direction. (The randomly dispersed red dots seen in the microchannels with V₁ and V₂ at 0 V arise due to scattering of the laser light from a non-ideal alignment of the liquid crystals.) **b**, Laser spectra measured for laser light transmission through LC₂ as a function of V₂.

approach that facilitates directional intensity control within a full 2π radians.

Thus far, the hollow microchannels (Fig. 2b) have been empty, but we now take advantage of them by infiltrating them with liquid crystals to create a novel hybrid fibre device capable of modulating the coherent laser emission as a function of angle. The linearly polarized annular wavefront escaping the PBG cavity simultaneously interacts with the multiple liquid-crystal microchannels surrounding it, each of which can be independently controlled. In the absence of an applied electric field, the liquid-crystal director points along the microchannel axis. Applying a potential difference across an electrode pair flanking a liquid-crystal-infiltrated microchannel generates an electric field perpendicular to the liquid-crystal director. Above a threshold voltage, the applied field produces a torque on the liquid-crystal molecules that leads to their rotation²⁸. The optical anisotropy of liquid-crystal molecules, together with control of their spatial orientation, provides a mechanism with which to continuously modify the linearly polarized state of the laser light passing through each microchannel. By

fixing a thin external linear polarizer around the fibre, this mechanism is used to modulate the azimuthal laser intensity distribution. We note that, although a whispering-gallery-like emission with a precise polarization state could also in principle be modulated by an annular array of liquid-crystal channels, the non-radial nature of this emission in the vicinity of the cavity would pose significant practical challenges to enable this oblique transmission to be efficiently modulated.

We demonstrate the principle of directional emission control by contacting two oppositely facing liquid-crystal microchannels to allow for simultaneous and independent tuning of the light intensity emitted from opposite sides of the same fibre (shown in Fig. 5a and described in the Methods). A R590-doped water plug is positioned in the core of the fibre and axially pumped as described previously. A thin polarizer sheet is wrapped around the fibre with its transmission axis aligned along the fibre axis so that the emitted light is blocked in the absence of an applied electric field or below the threshold voltage. Above the threshold voltage, independent intensity modulation of laser light passing through each liquid-crystal-filled microchannel is clearly visible in the images (left and

right sides of Fig. 5a) and is further substantiated by measuring the laser spectra as a function of driving voltage (Fig. 5b). The measurements reveal a maximum extinction ratio of ~ 9 dB.

The precise control over the omnidirectional intensity distribution from the surface of a thin and flexible fibre suggests a wide range of intriguing opportunities. The ability to introduce a directionally emitting laser catheter into a blood vessel could enable spatial and angularly selective irradiation of diseased sections while sparing healthy tissue (Supplementary Fig. S1) in conjunction with treatments such as photodynamic therapy²⁹. A lab-in-a-fibre application would involve using the fibre laser to interrogate fluids in the adjacent microchannels. Finally, the integration of a modulator and light source in a single fibre represents an important step towards the realization of flexible and directional fabric displays (Supplementary Fig. S2).

Methods

Fibre fabrication. The multilayer film was fabricated by thermal evaporation of a 4- μm -thick $\text{As}_{25}\text{S}_{75}$ layer onto each side of a 10- μm -thick polycarbonate (Lexan) film. This film was subsequently rolled onto a Teflon-lined mandrel and additional thicker polycarbonate films added to increase the outer diameter to 30 mm, after which this preform was consolidated under vacuum at ~ 190 °C until the individual layers fused together into one solid part. After consolidation, groups of three pockets with prescribed dimensions were machined along the length of the preform. The two outer pockets were filled with CPE strips and the centre pocket left empty. Additional polycarbonate films were rolled around the preform to a diameter of 40 mm, followed by a second consolidation step. During the subsequent thermal drawing process, the preform was scaled down by a factor of ~ 100 , resulting in the vacant pockets being pulled into hollow microchannels, the CPE strips being drawn into continuous electrodes (to be contacted post draw), and the multilayer glass/polymer microstructure being drawn into a nanostructured optical cavity lining the inner core of the fibre.

Microfluidic controls. Bidirectional pumping of fluid into and out of the fibre was achieved by alternating the electrical actuation of microdispensing valves (Lee Company VHS M/2) connected to pressurized and depressurized silicone oil reservoirs. Depressurization was achieved using a standard Venturi-based vacuum generator.

Laser characterization. The organic laser dye Rhodamine 590 (Exciton), dissolved in deionized water at a concentration of 1 mM, was infiltrated into the fibre core with a syringe. The pump beam from the second harmonic (532 nm) of a linearly polarized Nd:YAG laser (Continuum Minilite II) with a nominal pulse duration of 9 ns and 10 Hz repetition rate was coupled into the fibre core through a lens with a focal length of 10 cm. A small fraction of the pump beam was diverted with a beam splitter to monitor the input pump energy using a laser energy meter (Moletron EPM 1000 with the J4-09 probe). A $\times 10$ objective lens was used to collect a fraction of the light emitted radially from the fibre and focused directly onto the entrance slit of a spectrometer (Ocean Optics USB4000-UV-VIS). The polarization of the emitted light was measured by rotating a linear polarizer positioned between the fibre and the spectrometer.

Intensity modulation using liquid crystals. Liquid crystals (Merck MLC-2058) were introduced into the microchannels by capillary action, resulting in the liquid-crystal director aligning parallel to the fibre axis. A function generator (Stanford Research Systems DS345) operated at a sinusoidal 100 Hz was used to drive a high-voltage amplifier (A.A. Lab Systems A-301), which was connected to the electrodes. A $\times 10$ objective lens was used to image each liquid-crystal-filled microchannel to a charge-coupled device (CCD) camera (Motic Moticam 1000). A series of images were recorded as the voltage was changed. The CCD camera was replaced with a spectrometer to measure the laser spectra.

Received 4 October 2011; accepted 4 January 2012;
published online 11 March 2012

References

- Chang, R. K. & Campillo, A. J. *Optical Processes in Microcavities* (World Scientific, 1996).
- McCall, S. L., Levi, A. F. J., Slusher, R. E., Pearson, S. J. & Logan, R. A. Whispering-gallery mode microdisk lasers. *Appl. Phys. Lett.* **60**, 289–291 (1992).
- Knight, J. C., Driver, H. S. T., Hutcheon, R. J. & Robertson, G. N. Core-resonance capillary-fiber whispering-gallery-mode laser. *Opt. Lett.* **17**, 1280–1282 (1992).
- Kawabe, Y. *et al.* Whispering-gallery-mode microring laser using a conjugated polymer. *Appl. Phys. Lett.* **72**, 141–143 (1998).
- Moon, H.-J., Chough, Y.-T. & Kyungwon, A. Cylindrical microcavity laser based on the evanescent-wave-coupled gain. *Phys. Rev. Lett.* **85**, 3161–3164 (2000).
- Malko, A. V. *et al.* From amplified spontaneous emission to microring lasing using nanocrystal quantum dot solids. *Appl. Phys. Lett.* **81**, 1303–1305 (2002).
- Kazes, M., Lewis, D. Y., Ebenstein, Y., Mokari, T. & Banin, U. Lasing from semiconductor quantum rods in a cylindrical microcavity. *Adv. Mater.* **14**, 317–321 (2002).
- Yeh, P., Yariv, A. & Marom, E. Theory of Bragg fiber. *J. Opt. Soc. Am.* **68**, 1196–1201 (1978).
- Ball, G. A. & Morey, W. W. Continuously tunable single-mode erbium fiber laser. *Opt. Lett.* **17**, 420–422 (1992).
- Dianov, E. M., Likhachev, M. E., Fevrier, S. Solid-core photonic bandgap fibers for high-power fiber lasers. *IEEE J. Sel. Top. Quantum Electron.* **15**, 20–29 (2009).
- Wu, C. *et al.* Optically pumped surface-emitting DFB GaInAsP/InP lasers with circular grating. *Electron. Lett.* **27**, 1819–1820 (1991).
- Erdogan, T. *et al.* Circularly symmetric operation of a concentric-circle-grating, surface-emitting, AlGaAs/GaAs quantum-well semiconductor laser. *Appl. Phys. Lett.* **60**, 1921–1923 (1992).
- Labilloy, D. *et al.* High-finesse disk microcavity based on a circular Bragg reflector. *Appl. Phys. Lett.* **73**, 1314–1316 (1998).
- Scheuer, J., Green, W. M. J., DeRose, G. & Yariv, A., Low-threshold two-dimensional annular Bragg lasers. *Opt. Lett.* **29**, 2641–2643 (2004).
- Abouraddy, A. F. *et al.* Towards multimaterial multifunctional fibres that see, hear, sense and communicate. *Nature Mater.* **6**, 336–347 (2007).
- Ruff, Z. *et al.* Polymer-composite fibers for transmitting high peak power pulses at 1.55 microns. *Opt. Express* **18**, 15697–15703 (2010).
- Alkeskjold, T. T. *et al.* Integrating liquid crystal-based optical devices in photonic crystal fibers. *Opt. Quant. Electron.* **39**, 1009–1019 (2007).
- Kuhlmeiy, B. T., Eggleton, B. J. & Wu, D. K. C. Fluid-filled solid-core photonic bandgap fibers. *J. Lightwave Technol.* **27**, 1617–1630 (2009).
- Shapira, O. *et al.* Surface-emitting fiber lasers. *Opt. Express* **14**, 3929–3935 (2006).
- Eichler, H. J., Klein, U. & Langhans, D. Measurement of orientational relaxation times of Rhodamine 6G with a streak camera. *Chem. Phys. Lett.* **67**, 21–23 (1979).
- Duarte, F. J. & Hillman, L. W. *Dye Laser Principles* (Academic Press, 1990).
- Scifres, D. R., Streifer, W. & Burnham, R. D. Beam scanning with twin-stripe injection lasers. *Appl. Phys. Lett.* **33**, 702–704 (1978).
- McManamon, P. F. *et al.* Optical phased array technology. *Proc. IEEE* **84**, 268–298 (1996).
- Wang, X., Wilson, D., Muller, R., Maker, P. & Psaltis, D. Liquid-crystal blazed-grating beam deflector. *Appl. Opt.* **39**, 6545–6555 (2000).
- Choi, M., Tanaka, T., Fukushima, T. & Harayama, T. Control of directional emission in quasistadium microcavity laser diodes with two electrodes. *Appl. Phys. Lett.* **88**, 211110 (2006).
- Smith, N. R., Abeyinghe, D. C., Haus, J. W. & Heikenfeld, J. Agile wide-angle beam steering with electrowetting micropisms. *Opt. Express* **14**, 6557–6563 (2006).
- Kurosaka, Y. *et al.* On-chip beam-steering photonic-crystal lasers. *Nature Photon.* **4**, 447–450 (2010).
- Yeh, P. & Gu, C. *Optics of Liquid Crystal Displays* 2nd edn (John Wiley & Sons, 2010).
- Dolmans, D. E., Fukumura, D. & Jain, R. K. Photodynamic therapy for cancer. *Nature Rev. Cancer* **3**, 380–387 (2003).
- Rowland, K. J., Afshar, S., Stolyarov, A., Fink, Y. & Monro, T. M. Bragg waveguides with low-index liquid cores. *Opt. Express* **20**, 48–62 (2012).

Acknowledgements

A.M.S. is grateful to F. Capasso, A.F. Abouraddy, H. Stone, Z. Wang, D. Shemuly, S. Danto, D. Deng, Z. Ruff, N. Orf and A. Nemiroski for fruitful discussions. The authors thank M. Stolyar for his help in engineering the first rapid prototype version of the fluidic/optical-fibre coupler, and A. Gallant at the MIT Central Machine Shop for producing the final version. J. Ryvkina is credited for the artwork in Supplementary Fig. S2. A.M.S. acknowledges support from the US National Science Foundation Graduate Research Fellowship. L.W. acknowledges support from the Technical University of Denmark. This work was supported in part by the Materials Research Science and Engineering Program of the US National Science Foundation (award no. DMR-0819762) and also in part by the US Army Research Office through the Institute for Soldier Nanotechnologies (contract no. W911NF-07-D-0004).

Author contributions

A.M.S., L.W. and O.S. planned the experiments. A.M.S. and L.W. performed the experiments. A.M.S., L.W. and F.S. designed the fibre structures. A.M.S. and L.W. fabricated the fibres. O.S. and S.L.C. carried out simulations. A.M.S., L.W., O.S., F.S., Y.F. and J.D.J. conceived the ideas. A.M.S., J.D.J. and Y.F. co-wrote the manuscript. J.D.J. and Y.F. supervised the research. All authors analysed the data.

Additional information

The authors declare no competing financial interests. Supplementary information accompanies this paper at www.nature.com/naturephotonics. Reprints and permission information is available online at <http://www.nature.com/reprints>. Correspondence and requests for materials should be addressed to Y.F.